Accessing Carbon, Boron and Germanium Spiro Stereocenters in a Unified Catalytic Enantioselective Approach

Authors: Yi-Xuan Cao[1], Anne-Sophie Chauvin[2], Shuo Tong[3], Layth Alama[1], Nicolai Cramer[1]*

Affiliations:

[1] Laboratory of Asymmetric Catalysis and Synthesis, Institute of Chemical Sciences and Engineering, Ecole Polytechnic Fédérale de Lausanne, 1015 Lausanne, Switzerland.

[2] Group of Coordination Chemistry, Institute of Chemical Sciences and Engineering, École Polytechnique Fédérale de Lausanne 1015 Lausanne, Switzerland.

[3] MOE Key Laboratory of Bioorganic Phosphorus and Chemical Biology, Department of Chemistry, Tsinghua University, Beijing, 100084, China.

*Corresponding author. Email: nicolai.cramer@epfl.ch.

Abstract:

Achieving substrate generality in asymmetric catalysis is a long-standing goal, particularly for the selective construction of chiral heteroatoms. Compared to carbon, sulfur, phosphorus and silicon stereogenic centers, the methods for their boron and germanium congeners remain very scarce. Chiral (hetero) spirocycles are of relevance in several research domains. Methods effective for constructing carbon-centered chiral spirocycles do not translate to boron and germanium, leaving these chiral centers unexplored. We describe a unified strategy for constructing carbon, boron, and germanium-centered chiral spirocyclic skeletons *via* enantioselective hetero [2+2+2] cycloaddition of a *bis*-alkyne with a nitrile. A chiral designer Ni(0)NHC complex enables the required long-range enantioinduction. The resulting enantio-enriched spirocycles feature a pyridine motif, making them exploitable for ligand design and functional materials featuring attractive photophysical and chiroptical properties.

One sentence summary: A chiral designer Ni(0)-NHC complex catalyzes enantioselective hetero [2+2+2] cycloadditions in a unified approach to construct carbon, boron, and germanium-centered chiral spiro skeletons.

Main Text

Introduction: Developing substrate generality is a central aim and grand challenge in asymmetric catalysis, (*1*, *2*) particularly in constructing quaternary stereogenic centers and analogous main group heteroatom-stereogenic centers. Methods for their assembly have gained great attention due to their intriguing chemical, physical, biological, and stereoelectronic properties (**Fig 1A**). (*3*) For instance, carbon, boron, and germanium-centered chiral spirocycles are frequently found in chiral ligand design, (*4*) biologically active compounds, (*5*) and materials (**Fig 1B**). (*6*-*10*) Typically, accessing different chiral central elements requires distinctive synthetic strategies. In contrast to the recent advances to catalytically construct sulfur, (*11*) phosphorus (*12*) and silicon (*13*) stereogenic centers, methods to access other hetero-element stereocenters, namely boron (*14*) and germanium (*15*, *16*) remains so far largely underdeveloped due to unique synthetic challenges. For instance, tetracoordinate boron compounds possess a dative bond resulting in distorted tetrahedral geometry (*17*) and has potential lability. The longer as well as more labile germanium-carbon bonds in organo germanium compounds feature an enlarged tetrahedral geometry (**Fig 1A**). (*18*) These differences render most current strategies for the constructing of C, S, P, and Si stereogenic centers inapplicable for their B and Ge congeners. Despite considerable efforts to explore the

structural diversity of C, B, Ge centered spirocycles, it remains notoriously difficult to construct these chiral spirocyclic skeletons, particularly in a *unified strategy* or in an enantioselective manner. Methods to construct carbon-centered chiral spirocycles typically involve direct bond formations at the spirocenter. An enantioselective construction is achieved by differentiating functional groups near the spiro carbon atom *via* proximal stereocontrol (**Fig. 1C**). (*19*, *20*) The performance of the chiral catalysts is generally restricted to specific quaternary chiral spiro centers, often resulting in limited scope and reduced applicability. There are additional drawbacks in the construction of scaffolds featuring multiple functionalities where stereochemical information extends far from the spirocenter. (*21*, *22*) Accessing such elaborate chiral spirocyclic skeletons usually require lengthy routes such as modifying synthesized prochiral spirocycles, (*20*) or racemate resolution *via* chiral high-performance liquid chromatography (HPLC). (*23*) Moreover, established strategies cannot simply be extended to access chiral spirocycles with different central hetero atoms such as boron and germanium due to their unique and different reactivities (**Fig. 1A** & **1C**). Obtaining these enantioenriched products rely on nucleophilic substitutions and racemate resolution *via* chiral HPLC. (*24*, *25*) Therefore, the enantioselective construction of boron and germanium-centered chiral spiro skeletons remains a formidable challenge.

A key challenge in the development of a unified strategy for the construction of carbon, boron, and germanium-centered spirocyclic skeletons lies in the identification of a method of stereocontrol tolerant to distinctive tetrahedral geometries of the spirocyclic center and to diverse functionalities. A remote desymmetrizing ring closure appeared to us as promising strategy to construct the targeted chiral spirocycles. Such approach involves introducing an enantiotopic *bis*-substitution on the carbon, boron, and germanium-based cyclic substrates. The enantioselective ring closure involving both enantiotopic substituents selectively create the spiro stereogenic center at a remote position (**Fig 1D**). Examples for such strategies for the asymmetric construction of spirocycles are rare (*26*, *27*) and exhibit largely limited scope. We looked to transition-metal-catalyzed [2+2+2] cycloadditions (*28*-*30*) as exploitable strategy for the desymmetrizing ring closure *via* arene formation. Integrating chiral spiro-skeletons formation with the formation of a pyridine from two alkynes and a nitrile bears significant value. The pyridine motif substantially enhances utility by an involvement of this group in downstream applications in ligand or material design. (*31*, *32*) Therefore, we considered an enantioselective hetero [2+2+2] cycloaddition (*33*-*35*) of two distal enantiotopic *bis*-alkynes with a nitrile as a promising strategy for constructing chiral spiro-skeletons if three key challenges could be addressed (**Fig 1D**). Firstly, the different side reactions of the *bis*-alkyne substrates such as alkyne cyclotrimerization or oligomerization needs to be suppressed. (*36*) Secondly, since the stereo-differencing element is remote from the hetero [2+2+2] cycloaddition reaction site, a chiral catalyst with the ability for efficient enantio-discrimination between the distal enantiotopic alkynes is required. (*37*) Thirdly, the catalyst needs to accommodate the distorted and enlarged geometries of the boron and germanium centers as well as work under mild reaction conditions to ensure survivability of these more fragile bonds. Leveraging our experience in designing and applying chiral NHCs in asymmetric catalysis, (*38*, *39*) we prepared a C_2-symmetric chiral Ni(0)NHC styrene complexes able to selectively catalyze hetero [2+2+2] cycloadditions assembling carbon-, boron- and germanium-centered spirocyclic skeletons *via* a long-range enantioinductions. Mechanistic insights point towards a heterocoupling mechanism and allow for insight into the enantiodetermining step. Moreover, the rapid assembly of complex chiral compounds with attractive photophysical and chiroptical properties underscore the applicability for functional materials.

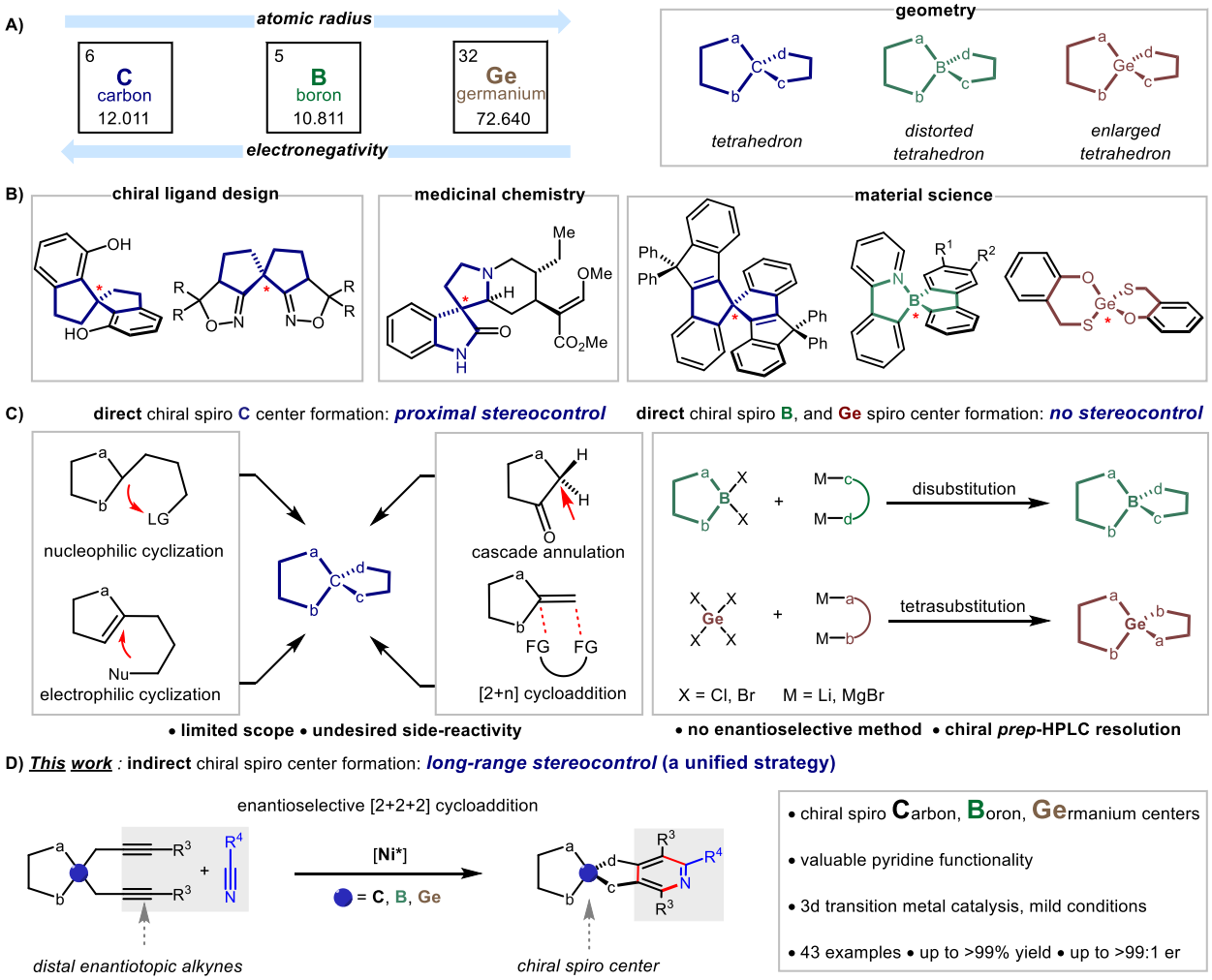

Fig 1. Catalytic enantioselective construction of chiral spirocyclic skeletons. A). Distinctive chemical-physical properties of carbon, boron, and germanium-centered chiral spiro skeletons. B). Examples of applications of chiral spirocycles in different fields. C). Established methodologies and challenges for enantioselective construction of chiral spirocycles. D). Present work: nickel-catalyzed enantioselective hetero [2+2+2] cycloaddition for remote construction of chiral spirocycles.

Development of the enantioselective hetero [2+2+2] cycloaddition: Incorporating rigidity stemming chiral spirocycles in proximity to exploitable motifs often used for materials such as fluorene is highly desirable. (*40*) Thus, fluorene substrate **1a** and benzonitrile were selected as substrates for the targeted hetero [2+2+2] cycloaddition. Employing just 3 mol% of chiral catalyst **Ni1** with a simple saturated ethylene bridge resulted in the formation of product **7** in excellent yield but with a very low level of enantioinduction (**Fig 2**). By installing the acenaphthylene backbone (**Ni2**), we observed an improvement in catalysis performance and product **7** was formed with 70:30 er (**Fig 2**). Catalyst **Ni3** which incorporated fluorine atoms into the chiral sidearms further enhanced catalyst performance and gave **7** in 95 % yield and a selectivity of 92:8 er. (**Fig 2**). To gain a better understanding of how steric and electronic modulation in nickel-NHC complex influence enantioselectivity, we analyzed the crystal structures of **Ni1**, (*41*) **Ni2**, and **Ni3**. The chiral-side arm of **Ni1** complex is relatively flexible. Compared to **Ni2** and **Ni3**, it has a different chiral pocket and less buried volume. However, we observed no substantial visual differences in the chiral pockets of **Ni2** and **Ni3**. Furthermore, attempts to improve the design of **Ni2**, an incorporation of 3,5-dimethyl substituents to enhance

the steric bulk of the chiral side arm resulted in a substantial drop yield, without improvement in enantioselectivity (**Table S2**, **L7**). Thus, it became evident that simply a more confined microenvironment is unlikely to improve selectivity. Regarding electronic effects, weak π-π stacking was observed between the chiral side arm and the acenaphthylene motif in **Ni2** complex (**Fig. S1-S4**), reducing the flexibility of the chiral sidearm. In total, 6 different molecules of **Ni2** complex appear in the unit cell of the crystal (**Fig. S1**). These variations at the distance between the chiral sidearms and the acenaphthylene backbone, indicating that the flexibility of the chiral side arms might be still relevant (**Fig. S2-S4**). The electron density of the chiral sidearm in **Ni3** complex was effectively reduced by the introduction of 3,5-difluoro substituents. This modulation resulted in stronger π-π stacking with the acenaphthylene backbone establishing a more defined chiral environment as depicted in the crystal structure of **Ni3** (**Fig. S5**, **S6**). These findings underscore that a chiral sidearm displaying rigidity and stability to the C_2 symmetric chiral environment is of strong relevance for achieving high levels of enantioinduction. Detailed reaction condition optimizations are available in **Table S1-S8**.

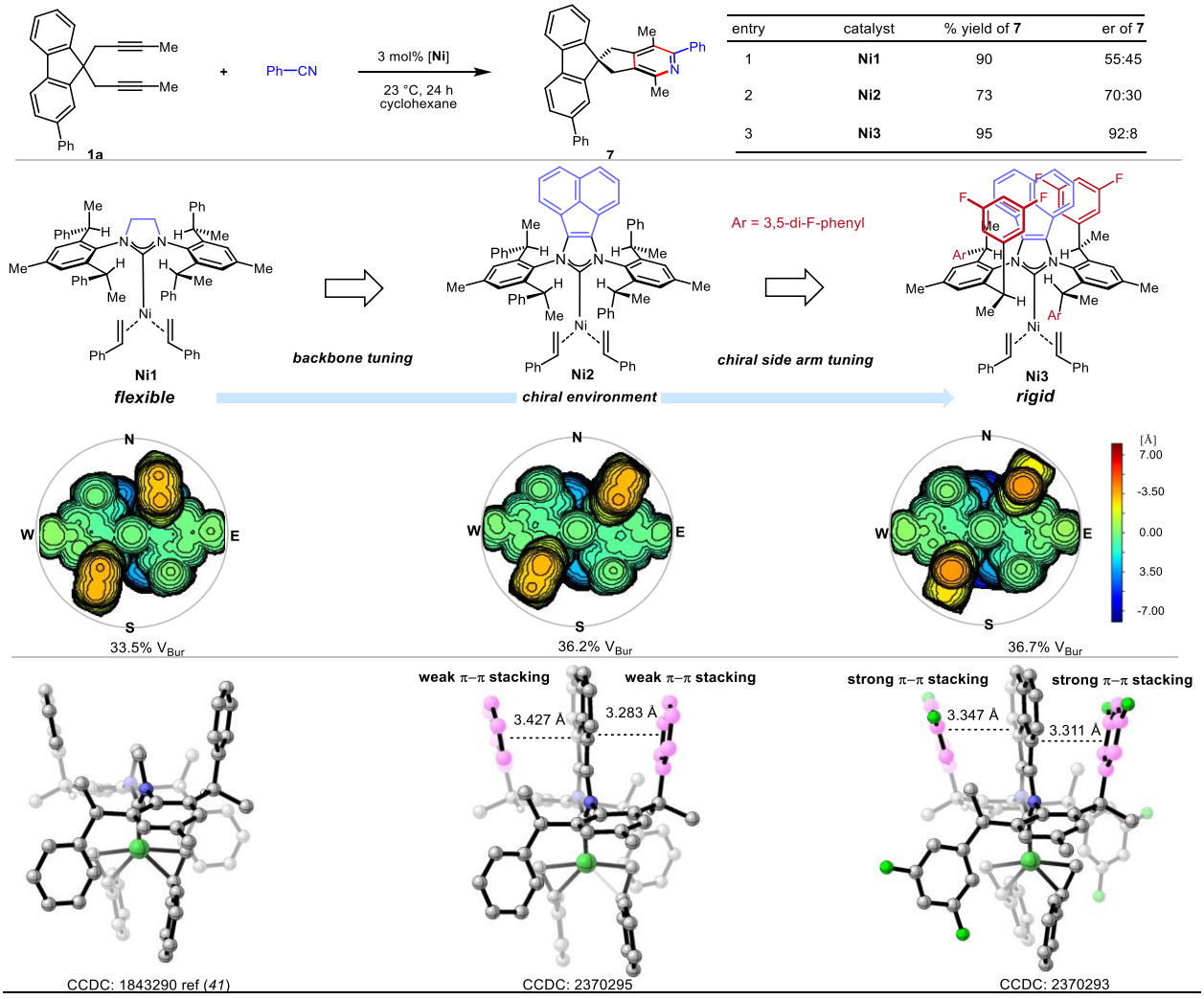

Fig 2. Catalyst development for enantioselective construction of chiral spiro-skeleton. Non-stereogenic hydrogen atoms are omitted for clarity.

Substrate scope of the enantioselective hetero [2+2+2] cycloaddition: With the optimized catalyst and conditions, we first investigated the reactivity and selectivity of different aromatic nitriles in the process (**Fig. 3**). In this respect, both electron-donating groups (-OMe, -NMe_2) and electron-withdrawing groups (-CF_3, -F) were accommodated, providing the corresponding

pyridines **8a** to **8e** in high yields and enantioselectivities. The process is mild and displays a good functional group tolerance, allowing incorporation of ester, pinacol boryl, chloro-, and vinyl groups as substituent on the nitriles (**8f** to **8i**). Similarly, reactions with aliphatic nitriles including acetonitrile, phenyl acetonitrile, valeronitrile, cyclopropanecarbonitrile, and 3-methoxy propionitrile provided pyridines **8j-8n** in high enantioselectivities. X-ray crystallographic analysis of pyridine **8m** allowed determination of its absolute configuration. Hept-6-ene-nitrile possessing a terminal olefin moiety cleanly gave **8o** in 88% yield and a 98:2 er with no chain-walking products involving the olefin detected. (*39*) Electron-rich heteroaromatic nitriles such as 3-cyanothiophene and *N*-Me-2-cyano pyrrole yielded pyridines **8p** (90% and 98.5:1.5 er) and **8r** (73% and 97:3 er). 2-Cyanopyridine as example for an electron-poor heterocycle is particularly noteworthy that product **8q** features the sought-after 2,2'-bipyridine motif. (*32*) Cyano ferrocene was also effectively accommodated without catalyst poisoning or side-product formation. Concerning the alkyne pattern, ethyl substituents resulted in a similar outcome (**8u**). The challenging terminal dialkyne produced the desired desymmetrization product **8t**, albeit in somewhat reduced enantioselectivity. Functionalized *bis*-1,4-enyne **1i** and *bis*-1,3-enyne **1k** engaged in the hetero [2+2+2] cycloaddition yielding *bis*-olefin bearing pyridines **8v** and **8w** that could be exploited for subsequent polymerization reactions. (*42*) Variations on fluorene core substituent R^1 include different aryl groups (**8y** and **8z**) and a *bis*-PMP amino group (**8x**) that has prominent appearances in spirofluorene materials.[40] Notably, installing a pinacol boryl group at R^1 gave pyridine **8aa** which can act as broadly diversifiable intermediate *via* a variety of cross-couplings. Next, we aimed to explore the suitability of enantioselective hetero [2+2+2] cycloaddition for generating spiro hetero-atom chirality. In this respect, an extension of the process to chiral tetra-coordinated boron compounds (*10*) focusing on the aza-borafluorene was initially followed. Pleasingly, under same reaction conditions **Ni3** displayed a robust performance and delivered pyridine derivatives **9a** and **9b** with their boron stereogenic centers in excellent yields and very good enantioselectivity. A slight erosion of selectivity was found for products **9c** and **9d** which have a relatively smaller substituent R^5. Interestingly, the effect of the distorted tetrahedral geometry of the boron starting material manifests itself by different selectivities of substrates that are identical besides having the *bis*-phenyl amino substituent on the phenyl ring (**9e**) or on the pyridine ring (**9b**), with the former providing a superior enantiomeric ratio. As for the previous carbon series, a diverse range of nitriles, including aromatic, aliphatic and heteroaromatic nitriles, was found to be compatible leading to corresponding chiral spiro boron compounds **9e** to **9g** in excellent enantioselectivities. 1-(4-(*t*Bu)phenyl)isoquinoline-based boron dialkyne substrate **3g** displaying a complex steric environment yielded pyridine **9h** in 84% yield and 95:5 er. A further extension was reached with *N*,*N'*-chelated boron scaffolds. (*43*) These pyridyl pyrrolide chelated boron substrates were amenable to the transformation and the corresponding spirocyclic tetra-coordinated boron compounds **9i** and **9j** were formed in excellent yield and moderate to good selectivities. Our focus shifted next to the selective construction of chiral spirogermanium center. Using germafluorene[9] **5a** (R^1=Ph) as a starting material provided spiro germafluorene **10a** in 85% yield albeit in virtually racemic form. Since phenyl as R^1 substituent was highly selective in the carbon as well as in the boron series, we attribute this lack of selectivity as direct result of the longer C-Ge bond length and its induced distortion of the center and altered vector of R^1. However, the selectivity of the transformation was restored with substrate **5b** (R^1=*t*Bu) leading to spiro germafluorene **10b** in 91% yield and 80:20 er. Furthermore, the reaction of **5c** (R^1=trityl) yielded compound **10c** increased in 95%

yield and an increased er of 86:14. Surprisingly, exposure of silicon-based analogues **4a** and **4b** to the reaction conditions caused substrate decomposition and the formation of pyridine products was not observed.

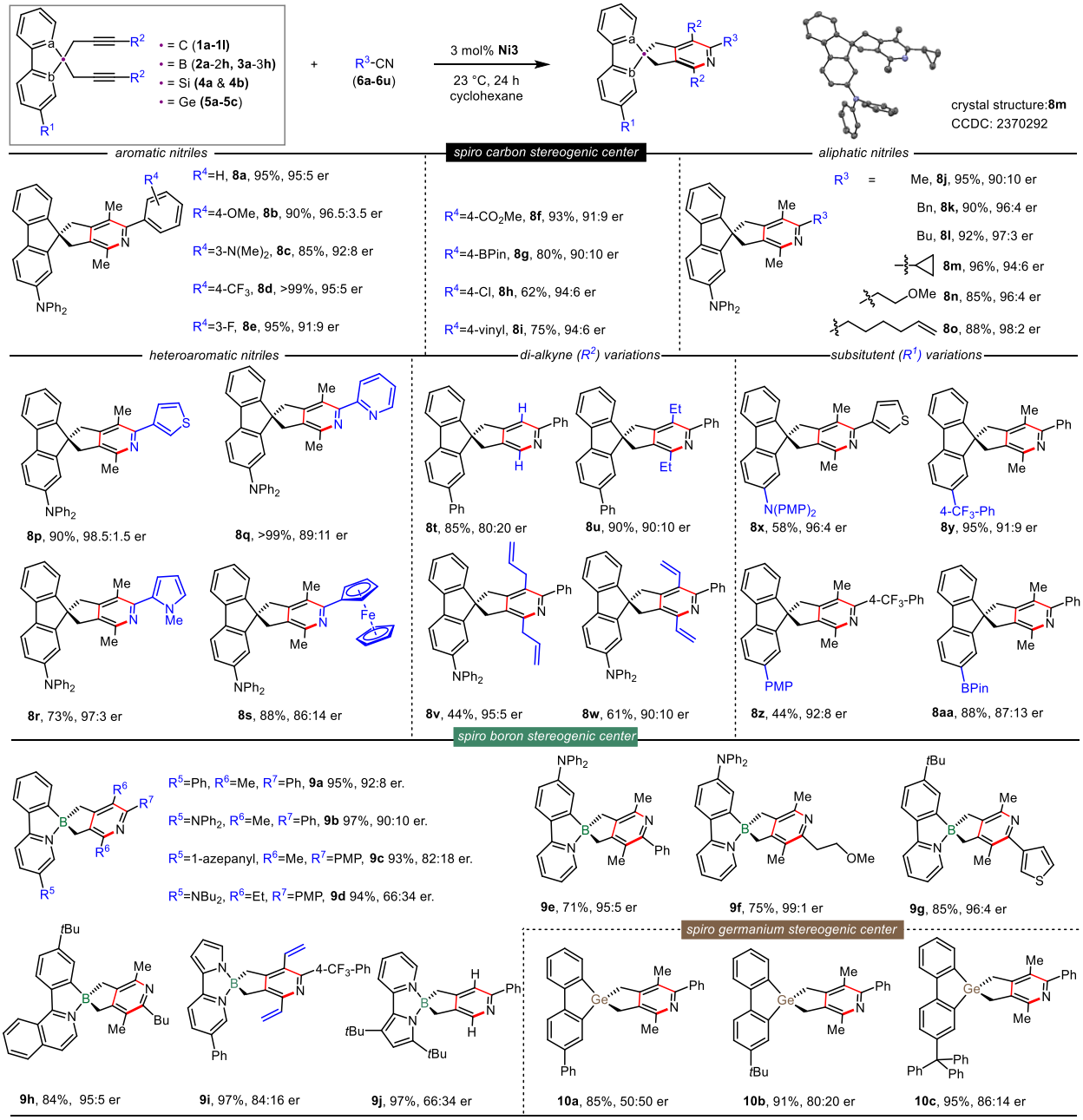

Fig 3. Scope of nickel-NHC-catalyzed enantioselective hetero [2+2+2] cycloaddition of chiral spiro skeletons construction. PMP = *p*-methoxy-phenyl.

Synthetic application of the chiral spirocycles: Given the wide-spread usage of bipyridines and 2-phenyl pyridines as ligands or ligand precursors, we reasoned that the obtained spirocycles can be connected to a metal center to impart intriguing material properties. (*23*, *32*) By utilizing products **8q** and **8b**, we rapidly accessed the chiral variants of widely applied copper-based light-emitting electrochemical cells (LEC) (*44*) and platinum-based organic light-emitting diodes (OLEDs) (*45*), **11a** and **11b**, respectively (**Fig. 4**). The luminescence properties of **11a** and **11b** were analyzed and fluorescence lifetimes and quantum yields

compared well with literature (**Fig. S8-S11**, **Table S9**). (*44*, *45*) To further showcase the utility of the process with complex molecules displaying intriguing chiroptical properties, we prepared a chiral C_2-symmetric *bis*-spiro fluorene **11c** with a highly conjugated heptacyclic core in a rapid synthetic sequence. *Bis*-pyridine **8ab** was prepared in 95% yield with an 87:13 dr and >99:1 er by a double enantioselective [2+2+2] heterocyclization of 1,4-dicyanobenzene with dialkyne **1d**. A double pyridine-directed electrophilic borylation gave tetrabromide **8ac**. Subsequent treatment of **8ac** with $AlMe_3$ exhaustively replaced all four bromides by methyl groups leading to compound **11c** in 50 % yield. The photophysical and advanced chiroptical properties of **11c** were measured. (**Fig. 4D**) The emission spectrum of **11c** ranges from 350 nm to 650 nm, with three prominent maxima, the maximum was blue shifted in solid state by ~2820 cm^{-1}. The fluorescence lifetimes of **11c** are on a microsecond scale which are similar to the known thermally activated delayed fluorescence (TADF) materials (**Table S9**). (*46*) Notably, compound **11c** exhibited an appreciable CPL activity, with a dissymmetric factor $|g_{lum}| = 1.5 \times 10^{-3}$ at 490 nm (**Fig. 4E** & **Fig. S12**). The value of the important dissymmetric factor of **11c** is of similar magnitude than the ones of existing chiral organic dyes as well as helicenes. (*47*, *48*)

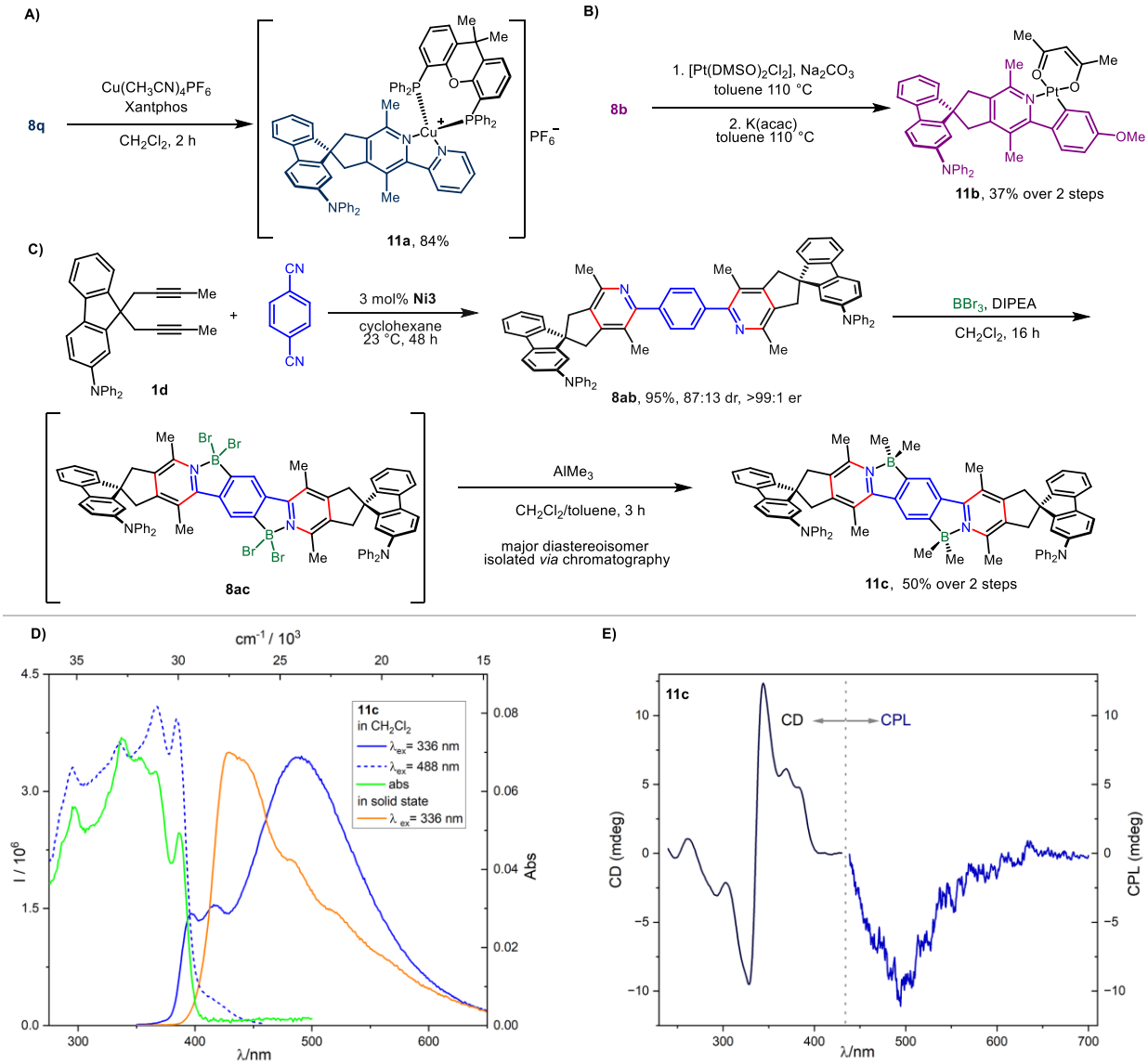

Fig 4. Synthetic applications. A). Synthesis of Cu(I) complex **11a**. B). Synthesis of Pt(II) complex **11b**. C). Synthesis boron compound **11c**. D). Corrected excitation (dot line), emission (plain line), and absorbance (green solid-line, y-right scale) of compound **11c** (1μM in CH_2Cl_2 or solid-state). E) *Circular dichroism* ***(***CD) and circularly polarized luminescence (CPL) spectra of **11c (**1μM in CH_2Cl_2).

Mechanistic studies: The hetero [2+2+2] cycloaddition between two alkynes and one nitrile could proceed either by *a*) a homocoupling mechanism in which the two alkynes link together first, or *b*) a heterocoupling mechanism in which one of the alkynes and the nitrile link together first. (*29*) Correlation with a previous report (*49*) suggests that the heterocoupling path is indeed operative. To shed some light to the interactions of the chiral Ni(0)NHC complex with the substrates, we synthesized Ni-nitrile complex **Ni4** *via* complexation of **L10** with $Ni(COD)_2$ and *p*-methoxybenzonitrile in 90 % yield (**Fig. 5A**). Evidenced by crystal structure analysis, **Ni4** exhibits a dimeric structure with planar geometry. Each nitrile binds to two nickel atoms in η^1 and η^2 modes. The R-C-N bond angle is changed from 180° of the former nitrile to 134.12° in the complex indicating substantial π-back-bonding, in line with a strong d^8 Ni(II) metallaazirene character. (*50*) **Ni4** is a competent catalyst and when used instead of **Ni3**, an identical reaction yield and enantiomeric ratio was observed (**Fig. S14**), suggesting that the styrene ligands of **Ni3** likely have a pure spectator role in the later catalytic cycles. No reaction occurred between precatalyst **Ni3** and *p*-methoxybenzonitrile (**Fig. 5B**), indicating that *a*) nickel has a stronger affinity to styrene than nitrile. *b*) coordination of the nitrile is contingent upon ligand exchange of styrene with alkyne substrate. Exposing **Ni4** to styrene did not result in formation of **Ni3**, but lead to complex decomposition instead (**Fig. 5B**). This behavior is further indicative of the Ni(II) character of **Ni4** species and suggests that the formation of the metallaazirene species is irreversible. (*49*) In the absence of a nitrile, **Ni3** cleanly catalyzes alkyne trimerization. However, in the presence of nitrile, the formation of pyridine is largely favored. This indicates that pyridine formation proceeds much faster than cyclotrimerization of alkyne (**Fig. 5C**). With the heterocoupling mechanism operative, the enantiodetermining step is the selective migratory insertion of one of the enantiotopic alkynes into the Ni(II) metallaazirene. The crystal structure of **Ni4** shows that the nitrile substrates are perfectly sandwiched in the middle of chiral side arms with a planar geometry (**Fig. 5**), suggesting that the chiral side arms of the carbene can effectively discern stereochemical information from the dialkyne substrate to achieve enantioselectivity. In sum, these observations enable us to propose a mechanism for the enantioselective hetero [2+2+2] cycloaddition (**Fig. 5D**). To initiate a first cycle, ligand exchange occurs on **Ni3**, whereas a dialkyne substrate and nitrile replace both styrenes yielding intermediate **I**. Subsequently, oxidative cyclization occurs, leading to the formation of a metallaazirene intermediate. An enantiodetermining migratory insertion of the coordinate alkyne towards the metallaazirene species proceeds. The orientation of group R^1 of the dialkyne substrate is paramount for the selectivity. The substituent R^3 on the nitrile has significantly less impact on the selectivity due to its distance from the chiral sidearm. The substrate catalyst complex adopts an orientation in which the substituent R^1 is favorably placed to the least hindered position leading preferentially to intermediate $\mathbf{II}^1$ over the more congested alternative orientations $\mathbf{II}^2$, $\mathbf{II}^3$, and $\mathbf{II}^4$. Following the migratory insertion step, the coordination of the second alkyne moiety leads to intermediate **III**. Subsequent second migratory insertion leads to the formation of a 7-membered metallacycle **IV**. Driven by aromatization, a facile reductive elimination forms the chiral spirocyclic pyridine matching the

obtained absolute configuration of **8m**. Coordination of the next set of substrates regenerates intermediate **I** and completes the catalytic cycle.

Conclusion: We reported a nickel-catalyzed pyridine-forming enantioselective hetero [2+2+2] cycloaddition as a unified approach for constructing chiral carbon-, boron-, and germanium-centered spiro-skeletons. The required remote stereocontrol is achieved by a designed chiral bulky NHC-Ni(0)-styrene complex. An electron-poor aryl group as chiral sidearm provides a strong π-π stacking with the ligand backbone creates a well-defined C_2-symmetric chiral pocket which proved to be pivotal for the induced selectivity of the catalyst. The reaction proceeds *via* a heterocoupling mechanism with the migratory insertion of an enantiotopic alkyne towards the metallaazirene species being the enantiodetermining step. Moreover, the technology is suitable for rapidly assemble highly complex compounds with attractive and exploitable photophysical and chiro-optical properties. The outlined method considerably enlarges the toolbox to assemble chiral functional materials and to construct boron and germanium heteroatom chirality.

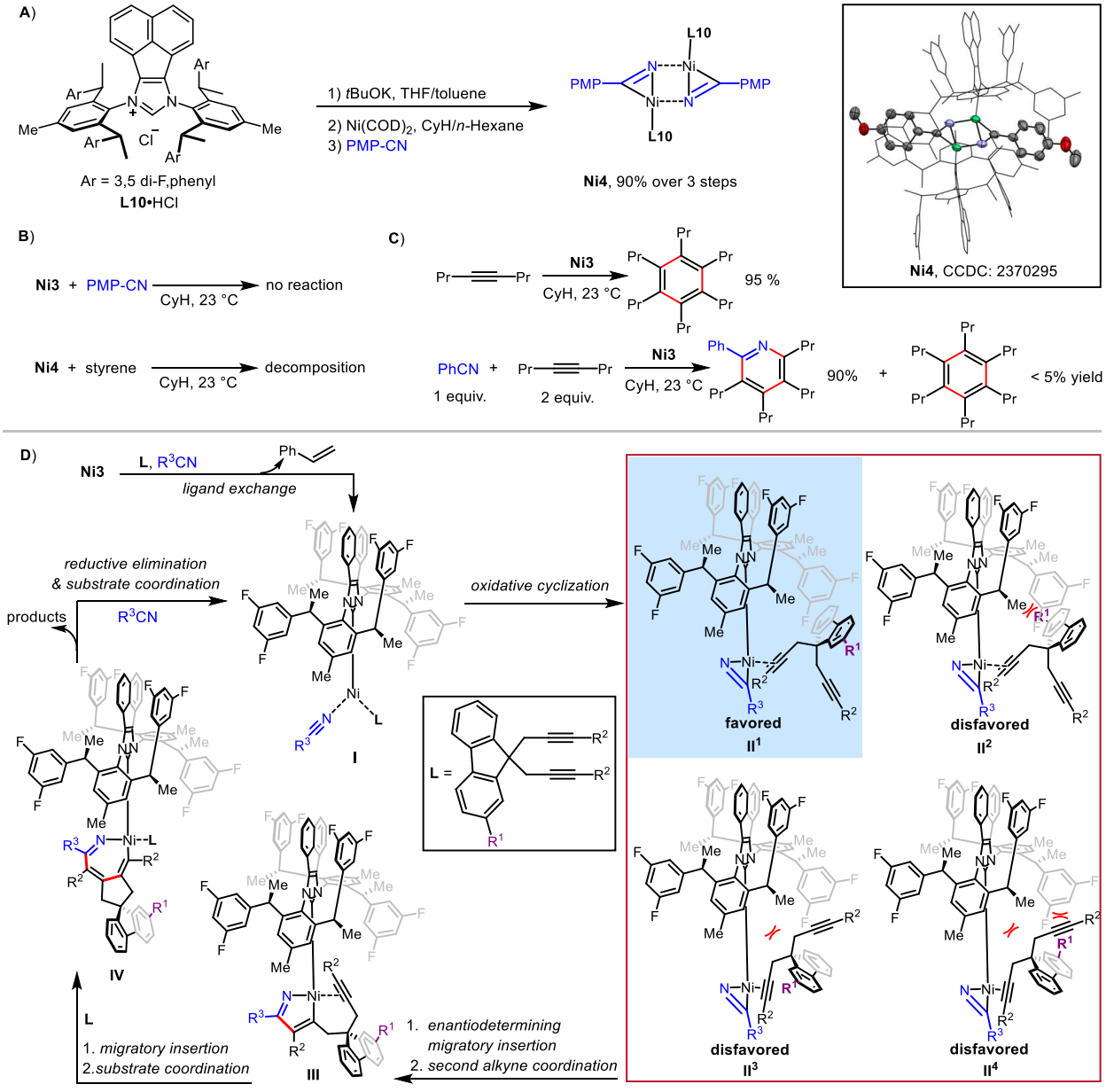

Fig 5. Mechanistic studies of Enantioselective Construction of Chiral Spirocycles. A). synthesis of nickel nitrile complex **Ni4**, ORTEP drawing of complex **Ni4 B**). Investigations of the nitrile coordination behavior in the presence of styrene. **C**). Comparison of pyridine formation rate versus alkyne cyclotrimerization rate. **D**). Suggested mechanism of Ni(0)NHC catalyzed enantioselective hetero [2+2+2] cycloaddition.

References and notes.

1. P. J. Walsh, M. C. Kozlowski, *Fundamentals of Asymmetric Catalysis* (Univ. Science Books, 2010).
2. C. C. Wagen, S. E. McMinn, E. E. Kwan, & E. N. Jacobsen, Screening for generality in asymmetric catalysis. *Nature* **610**, 680–686 (2022).
3. F. Pop, N. Zigon, N. Avarvari, Main-Group-Based Electro- and Photoactive Chiral Materials. *Chem. Rev.* **119**, 8435–8478 (2019).
4. K. Ding, Z. Han, Z. Wang, Spiro skeletons: a class of privileged structure for chiral ligand design. *Chem. Asian J.* **4**, 32–41 (2009).
5. Y. Zheng, C. M. Tice, S. B. Singh, The use of spirocyclic scaffolds in drug discovery. *Bioorganic & Medicinal Chemistry Letters*. **24**, 3673–3682 (2014).
6. T. P. I. Saragi, T. Spehr, A. Siebert, T. Fuhrmann-Lieker, J. Salbeck, Spiro compounds for organic optoelectronics. *Chem. Rev.* **107**, 1011–1065 (2007).
7. M. Grell, M. Oda, K. S. Whitehead, A. Asimakis, D. Neher, D. D. C. Bradley, A compact device for the efficient, electrically driven generation of highly circularly polarized light. *Adv. Mater*. **13**, 577–580 (2001).
8. S. Y. Yang, Y. K. Wang, C. C. Peng, Z. G. Wu, S. Yuan, Y. J. Yu, H. Li, T. T. Wang, H. C. Li, Y. X. Zheng, Z. Q. Jiang, L. S. Liao, Circularly Polarized Thermally Activated Delayed Fluorescence Emitters in Through-Space Charge Transfer on Asymmetric Spiro Skeletons. *J. Am. Chem. Soc.* **142**, 17756–17765 (2020).
9. O. Shynkaruk, G. He, R. McDonald, M. J. Ferguson, E. Rivard, Modular Synthesis of Spirocyclic Germafluorene-Germoles: A New Family of Tunable Luminogens. *Chem. Eur. J.* **22**, 248–257 (2016).
10. X. Li, G. Zhang, Q. Song, Recent advances in the construction of tetracoordinate boron compounds. *Chem. Commun*. **59**, 3812–3820 (2023).
11. S. Otocka, M. Kwiatkowska, L. Madalinska, P. Kielbasinski, Chiral Organosulfur Ligands/Catalysts with a Stereogenic SulfurAtom: Applications in Asymmetric Synthesis. *Chem. Rev.* **117**,4147−4181 (2017).
12. J. S. Harvey, V. Gouverneur, Catalytic EnantioselectiveSynthesis of P-Stereogenic Compounds. *Chem. Commun*. **46**, 7477−7485 (2010).
13. F. Ye, Z. Xu, L.-W. Xu, The Discovery of Multifunctional Chiral P Ligands for the Catalytic Construction of Quaternary Carbon/Silicon and Multiple Stereogenic Centers. *Acc. Chem. Res*. 54, 452−470 (2021).
14. B. Zu, Y. Guo, C. He, Catalytic Enantioselective Construction of Chiroptical Boron-Stereogenic Compounds. *J. Am. Chem. Soc*. **143**, 16302–16310 (2021).
15. A. C. Han, L. J. Xiao, Q. L. Zhou, Construction of Ge-Stereogenic Center by Desymmetric Carbene Insertion of Dihydrogermanes. *J. Am. Chem. Soc*. **146**, 5643–5649 (2024).
16. R. Shintani, C. Takagi, T. Ito, M. Naito, K. Nozaki, Rhodium-Catalyzed Asymmetric Synthesis of Silicon-Stereogenic Dibenzosiloles by Enantioselective [2 +2+2] Cycloaddition. *Angew.Chem., Int. Ed.* **54**, 1616−1620 (2015).
17. D. Li, H. Zhang, Y, Wang, Four-Coordinate Organoboron Compounds for Organic Light-Emitting Diodes (OLEDs). *Chem. Soc. Rev*. **42**, 8416−8433 (2013).

18. T. Rogova, E. Ahrweiler, M. D. Schoetz, F. Schoenebeck, Recent Developments with Organogermanes: their Preparation and Application in Synthesis and Catalysis. *Angew. Chem., Int. Ed.* No. e202314709 (2023).
19. R. Rios, "Enantioselective Synthesis of all Carbon Spiro Compounds" in *Spiro Compounds: Synthesis and Applications* (wiley, 2021), pp. 283–312.
20. P. W. Xu, J. S. Yu, C. Chen, Z. Y. Cao, F. Zhou, J. Zhou, Catalytic Enantioselective Construction of Spiro Quaternary Carbon Stereocenters. *ACS. Catal.* **9**, 1820–1882 (2019).
21. T. T. Talele, Opportunities for Tapping into Three-Dimensional Chemical Space through a Quaternary Carbon. *J. Med. Chem*. **63**, 13291–13315 (2020).
22. Y. Lou, J. Wei, M. Li, Y. Zhu, Distal Ionic Substrate-Catalyst Interactions Enable Long-Range Stereocontrol: Access to Remote Quaternary Stereocenters through a Desymmetrizing Suzuki-Miyaura Reaction. *J. Am. Chem. Soc*. **144**, 123–129 (2022).
23. H. Hamada, Y. Itabashi, R. Shang, E. Nakamura, Axially Chiral Spiro-Conjugated Carbon-Bridged p-Phenylenevinylene Congeners: Synthetic Design and Materials Properties. *J. Am. Chem. Soc.* **142**, 2059–2067 (2020).
24. Y. Yoshigoe, K. Hashizume, S. Saito, Synthesis and stereochemistry of chiral aza-boraspirobifluorenes with tetrahedral boron-stereogenic centers. *Dalton. Trans*. **42**, 17035–17039 (2022).
25. [1] P. Kitschke, T. Rüffer, H. Lang, A. A. Auer, M. Mehring, Chiral Spirocyclic Germanium Thiolates – An Evaluation of Their Suitability for Twin Polymerization based on A Combined Experimental and Theoretical Study. *ChemistrySelect*. **1**, 1184–1191 (2016).
26. Y.-F. Zhang, S.-J. Yin, M. Zhao, J.-Q. Zhang, H.-Y. Li and X.-W. Wang, Dinuclear Zinc-Catalyzed Desymmetric Intramolecular Aldolization: An Enantioselective Construction of Spiro[cyclohexanone-oxindole] Derivatives, *RSC Adv.* **6**, 30683–30689. (2016)
27. C. C. Shan, Z.-L. Wang, Y.-H. Xu, Copper-catalyzed desymmetric silylative-cyclization of 1,6-diynes for synthesis of spirocyclic compounds. *Org. Chem. Front*. **11**, 1211–1217. (2024)
28. P. Matton, S. Huvelle, M. Haddad, P. Phansavath, V. Ratovelomanana-Vidal, Recent Progress in Metal-Catalyzed [2+2+2] Cycloaddition Reactions. *Synthesis*. **54**, 4–32 (2022).
29. A. Roglans, A. Pla-Quintana, M. Solà, Mechanistic Studies of Transition-Metal-Catalyzed [2 + 2 + 2] Cycloaddition Reactions. *Chem. Rev*. **121**, 1894–1979 (2021).
30. M. Hapke, G. Hilt. Cobalt-catalyzed [2+2+2] cycloadditions. In Cobalt Catalysis in Organic Synthesis: Methods and Reactions, T. Gla¨ sel and M. Hapke, eds. (Wiley-VCH, 2022), pp. 287–335.
31. H. L. Kwong, H. L. Yeung, C. T. Yeung, W. S. Lee, C. S. Lee, W. L. Wong, Chiral pyridine-containing ligands in asymmetric catalysis. *Coordination Chemistry Reviews*. **251**, 2188–2222 (2007).
32. R. D. Costa, E. Ortí, H. J. Bolink, F. Monti, G. Accorsi, N. Armaroli, Luminescent ionic transition-metal complexes for light-emitting electrochemical cells. *Angew. Chem. In. Ed*. **51**, 8178–8211 (2012).
33. A. Link, C. Sparr, Stereoselective arene formation. *Chem. Soc. Rev*. **47**, 3804—3815 (2018).
34. H. Wang, B. Qiao, J. Zhu, H. Guo, Z. Zhang, K. Yang, S. J. Li, Y. Lan, Q. Song, Enantio- and regioselective [2 + 2 + 2] cycloaddition of BN-diynes for construction of C-B axial chirality. *Chem*. **10**, 317–329 (2024).

35. J. Cai, L. G. Bai, Y. Zhang, Z. K. Wang, F. Yao, J. H. Peng, W. Yan, Y. Wang, C. Zheng, W. B. Liu, Ni-catalyzed enantioselective [2 + 2 + 2] cycloaddition of malononitriles with alkynes. *Chem.* **7**, 799–811 (2021).
36. P. Bhatarah, E. H. Smith, S. Kensington, Nickel(0)-promoted Synthesis of Tetralin Lactones from the Monoynes and Octa-1,7-diynes Terminally Substituted with Groups Co-cyclisation of Ester or Amide groups *J. CHEM. SOC. PERKIN. TRANS*. 2163–2168 (1992).
37. X. P. Zeng, Z. Y. Cao, Y. H. Wang, F. Zhou, J. Zhou, Catalytic Enantioselective Desymmetrization Reactions to All-Carbon Quaternary Stereocenters. *Chem. Rev.* **116**, 7330–7396 (2016).
38. J. Diesel, A. M. Finogenova, N. Cramer, Nickel-Catalyzed Enantioselective Pyridone C-H Functionalizations Enabled by a Bulky N- Heterocyclic Carbene Ligand. *J. Am. Chem. Soc.* **140**, 4489–4493 (2018).
39. Y. X. Cao, M. D. Wodrich, N. Cramer, Nickel-catalyzed direct stereoselective α-allylation of ketones with non-conjugated dienes. *Nat. Commun.* **14**, 7640 (2023).
40. J. Shaya *et al.* Design, photophysical properties, and applications of fluorene-based fluorophores in two-photon fluorescence bioimaging: A review. *Journal of Photochemistry and Photobiology C: Photochemistry Reviews.* **52**, 100529. (2022)
41. Y. Cai, J. W. Zhang, F. Li, J. M. Liu, S. L. Shi, Nickel/N-Heterocyclic Carbene Complex-Catalyzed Enantioselective Redox-Neutral Coupling of Benzyl Alcohols and Alkynes to Allylic Alcohols. *ACS. Catal.* **9**, 1–6 (2019).
42. S. N. Hancock, N. Yuntawattana, S. M. Valdez, Q. Michaudel, Expedient synthesis and ring-opening metathesis polymerization of pyridinonorbornenes, *Polym. Chem.* **13**, 5530–5535 (2022).
43. T. Yang, N. Tang, Q. Wan, S.-F. Yin, R. Qiu, Recent Progress on Synthesis of *N*,*N*′-Chelate Organoboron Derivatives. *Molecules* ***26***, 1401. (2021)
44. S. Keller *et al*. Shine bright or live long: substituent effects in [Cu(N^N) (P^P)]+-based light-emitting electrochemical cells where N^N is a 6- substituted 2,2'-bipyridine. *J. Mater. Chem. C*. **4**, 3857–3871 (2016).
45. J. Brooks, Y. Babayan, S. Lamansky, P. I. Djurovich, I. Tsyba, R. Bau, M. E. Thompson, Synthesis and Characterization of Phosphorescent CyclometalatedPlatinum Complexes. *Inorg. Chem*. **41**, 3055– 3066 (2002).
46. M. Stanoppi, A. Lorbach, Boron-based donor-spiro-acceptor compounds exhibiting thermally activated delayed fluorescence (TADF). *Dalton Trans*. **47**, 10394–10398 (2018).
47. D. Zhang, M. Li and C. Chen, Recent advances in circularly polarized electroluminescence based on organic light-emitting diodes. *Chem. Soc. Rev*, **49**, 1331–1343 (2020).
48. S. M. Guo, S. Huh, M. Coehlo, S. Li, G. Pieters, O. Baudoin, A C–H activation-based enantioselective synthesis of lower carbo[*n*]helicenes. *Nat. Chem.* **15**, 872–880 (2023).
49. R. M. Stolley, H. A. Duong, J. Louie, Mechanistic evaluation of the Ni(IPr)2-catalyzed cycloaddition of alkynes and nitriles to afford pyridines: Evidence for the formation of a key η1-Ni(IPr)2(RCN) intermediate. *Organometallics*. **32**, 4952–4960 (2013).
50. J. N. Humke, R. G. Belli, E. E. Plasek, S. S. Kargbo, A. Q. Ansel, C. C. Roberts, Nickel binding enables isolation and reactivity of previously inaccessible 7-aza-2,3-indolynes. *Science*. **384**, 408–414 (2024).

Acknowledgments: We thank Dr. R. Scopelliti and Dr. F. Fadaei Tirani for X-ray crystallographic analysis of compounds **8m**, **Ni2**, **Ni3**, and **Ni4**. We thank Dr. Young Ye for proofreading the manuscript.

Funding: This work is supported by EPFL and the NCCR Catalysis. This publication was created as part of NCCR Catalysis (grant number 180544), a National Centre of Competence in Research funded by the Swiss National Science Foundation.

Author contributions: Y. C. and N. C. designed the experiments. Y. C. performed the experiments. A. C. performed photophysical properties measurements of compound **11a-c**. S.T. performed CD and CPL measurements of compound **11a-c**. L. A. synthesized compounds **f2**, **f4**, **1f**, **2i**, **1l**, **8y**, **8z** and **8aa**. All authors analyzed the data and drafted the manuscript.

Competing interests: The authors declare no conflict of interest.

Data and materials availability:

Supplementary Materials

Materials and Methods

Supplementary Text

Figs. S1 to S16

Table S1 to S9

References (*51-68*)